

SAR imaging of wave dispersion in Antarctic pancake ice and its use in measuring ice thickness

P. Wadhams,^{1,2} F. F. Parmiggiani,³ G. de Carolis,⁴ D. Desiderio,^{4,5} and M. J. Doble²

Received 23 April 2004; revised 12 June 2004; accepted 12 July 2004; published 7 August 2004.

[1] A synthetic aperture radar (SAR) image of the advancing winter marginal ice zone (MIZ) in the Antarctic, composed of frazil-pancake ice, has been analysed in a new way in order to test the predictions of a recently developed theory of wave dispersion in pancake ice which treats the ice as a viscous layer. In the image, obtained in April 2000, the structure of the wave spectrum in the MIZ and its change from the open-water spectrum are consistent with a pancake layer 24 cm thick. Intensive *in situ* measurements of the pancake ice in the MIZ 280 km W of the image location were made from FS *Polarstern* during a period covering the satellite imaging, and also yielded a mean ice thickness of 24 cm. We conclude that this technique gives realistic results for ice thickness, whereas earlier work based on a different dispersion theory (mass loading) tended to over-estimate thickness. After further validation, it is therefore possible that the SAR wave technique can become an accepted method for monitoring ice thickness in pancake icefields. **INDEX TERMS:** 4275

Oceanography: General: Remote sensing and electromagnetic processes (0689); 4207 Oceanography: General: Arctic and Antarctic oceanography; 4560 Oceanography: Physical: Surface waves and tides (1255); 4594 Oceanography: Physical: Instruments and techniques. **Citation:** Wadhams, P., F. F. Parmiggiani, G. de Carolis, D. Desiderio, and M. J. Doble (2004), SAR imaging of wave dispersion in Antarctic pancake ice and its use in measuring ice thickness, *Geophys. Res. Lett.*, 31, L15305, doi:10.1029/2004GL020340.

1. Introduction

[2] The technique of extracting valid directional wave spectra from subscenes of satellite SAR imagery is now well established. After initial studies which extracted the SAR spectrum without correction [Wadhams and Holt, 1991], more recent work begins with conversion of the raw SAR spectrum into a valid sea surface directional spectrum. Using two of these techniques, the Hasselmann inversion [Hasselmann *et al.*, 1996] and the cross-spectra inversion [Engen and Johnsen, 1995], the present authors have used SAR spectra to derive the change in wave

dispersion as a wave train enters frazil and pancake icefields [Wadhams *et al.*, 1999, 2002]. By tracking the peak of the spectrum through a succession of subscenes as the waves move into the icefield, and measuring the change in wave number of this component on crossing the ice edge, we were able to estimate the ice cover thickness through use of thickness-dependent dispersion theory.

[3] In all of these studies we found that mass-loading theory, the simplest and apparently most plausible model for wave dispersion in pancake ice [Wadhams, 1986], predicts greater ice thicknesses than are actually observed, i.e., the measured decrease in wavelength on entering the icefield is greater than would be expected on theoretical grounds. Various hypotheses were advanced for this discrepancy, e.g., the possibility that the effective frazil-pancake layer thickness is greater than that given by mass of ice per unit area of sea surface, since the slick might be mixed down into the water column by turbulence [Wadhams and Holt, 1991]. However, in direct observations that we made by underwater camera under frazil-pancake icefields in the Greenland Sea and Antarctic Ocean, we found no evidence of such mixing.

2. Use of a New Wave Dispersion Theory

[4] We concluded that mass loading theory itself may be inappropriate as a description of wave dispersion in frazil-pancake ice. We found that a recently developed model by Keller [1998], in which the frazil-pancake ice cover is treated as a layer of highly viscous fluid, offers a better description of wave dispersion and attenuation which could give us a new means of obtaining more accurate thickness estimates. At high frequencies (around 0.5–1 Hz), like other viscous models, the model actually predicts an increase in wavelength in ice, which fits laboratory experiments by Newyear and Martin [1999]. At more typical oceanic frequencies, however, the model predicts a wavelength decrease. The unknown parameter in the model is the equivalent kinematic viscosity ν of the ice layer; Newyear and Martin [1999] found that a value of $(3.0 \pm 0.25) \times 10^{-2} \text{ m}^2 \text{ s}^{-1}$ gave the best fit between data and tank experiments.

[5] To test this new theory, we developed a new inversion procedure and applied it to an ERS-2 SAR image (orbit 26128, frame 5013) obtained from the winter Antarctic ice edge in the region of 68°S 25°W on April 19 2000. Field data were obtained during April 16–19 from an ice edge region 280 km to the west by FS *Polarstern*. Figure 1 shows the image used, spanning a very clear ice edge, where the bright part of the image is the rough open sea and the darker part is frazil-pancake ice. The image was pre-processed, speckle filtered [Baraldi and Parmiggiani, 1995] and geo-referenced according to the method used in earlier studies

¹Department of Applied Mathematics and Theoretical Physics, University of Cambridge, Cambridge, UK.

²Scottish Association for Marine Science, Dunstaffnage Marine Laboratory, Oban, Scotland.

³Istituto di Scienze dell'Atmosfera e del Clima, Consiglio Nazionale delle Ricerche (ISAC-CNR), Bologna, Italy.

⁴Istituto di Studi sui Sistemi Intelligenti per l'Automazione, Consiglio Nazionale delle Ricerche (ISSIA-CNR), Bari, Italy.

⁵Carlo Gavazzi Space SpA, Milan, Italy.

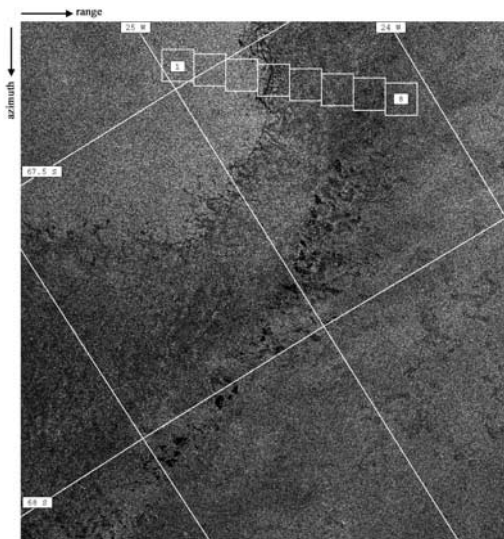


Figure 1. ERS-2 SAR image of Antarctic ice edge acquired on April 19, 2000 at 10:12 GMT (orbit 26128, frame 5013).

[Wadhams *et al.*, 2002]. While full resolution data were used for analyses, for display the scene was sub-sampled to 1000×1000 pixels (Figure 1). The inversion procedure was applied to 8 full resolution windows, or sub-scenes, 512×512 pixels in size, extracted from the SAR scene following the main direction of the waves as obtained from the observed SAR spectrum in the open sea. As the pixel size of full resolution data is 12.5 m, each box spans 6.4 km and the 8 boxes cover 51.2 km.

3. Spectral Inversion of the SAR Image in Open Water and Sea Ice

3.1. Open Water

[6] New inversion procedures were applied to both the open water and sea ice spectra. For open water the procedure estimates the wind-sea spectrum according to the parameterisation of Donelan *et al.* [1995; Mastenbroek and De Valk, 2000]. The parameters involved are wind speed and wave age, the latter defined as the ratio between wind speed and the phase velocity of the dominant wave. A preliminary estimation of the wind vector is therefore mandatory for a reliable inversion result. In this case the SAR image was used. The wind direction (with 180° ambiguity) was taken from the direction of windrows visible on the open sea area, which in this case appeared parallel to the range direction. The availability of QuikSCAT wind data gathered approximately two hours after the SAR passage allowed us to resolve the 180° ambiguity. QuikSCAT (Figure 2) measured a wind vector of about 6 m s^{-1} in magnitude blowing towards 121° . The ERS-2 platform was heading about 206° along a descending orbit so that the wind direction was 5° different to the range direction. This value compares well with the windrow direction detected on the SAR image. As a result, the true wind direction was taken as parallel to the SAR range direction, blowing toward E (SAR near range) where a

region covered by pancake ice is present. As the SAR image spectrum shows a wind-sea spectrum propagating along the range axis, we conclude that the wave train is penetrating *into* the ice zone from the open water. The wind speed at 10 m reference height U_{10} was estimated using both the CMOD-4 and CMOD-IFREMER models. The predicted values are 7.0 m s^{-1} and 8.5 m s^{-1} respectively. The speeds are consistent because they are within $\pm 2 \text{ m s}^{-1}$, which is the accuracy range of CMOD predictions. A further source of wind data which supports these values, although measured some 200 km away, was the wind sensor on one of the SAMS buoys (DML8), which gave a value of 5.5 m s^{-1} from 300° at that time.

[7] Given the wind vector, the inversion procedure searches for the wave age value $\Omega (=C_p/U_{10}$, where C_p is the phase speed of the peak wave) which minimises the difference between the observed and simulated SAR spectra. The simulation of the SAR spectrum is carried out using the integral transform given by Hasselmann and Hasselmann [1991]. A further minimisation is then carried out with respect to the propagation direction of the peak wave. In order to account for the microwave backscatter modulation as a result of surface tilt due to range-travelling waves, a preliminary estimation of the RAR (real aperture radar) modulation transfer function (MTF) was performed on the SAR image range profile. The modulus of the RAR MTF can be expressed as the slope $(\partial\sigma^\circ/\partial\theta)/\sigma^\circ$, where σ° is the backscatter coefficient and θ is the incidence angle. Its absolute value is 10.28, which is in good agreement with the theoretical value computed assuming a wave number spectrum decay k^{-4} and 23° as incidence angle.

[8] Assuming a wind speed of 8.5 m s^{-1} , the best-fit wind-generated wave spectrum in the open sea for the analysed SAR image gave the following:

Peak wavelength: 78 m

Peak direction: 42°

H_s : 1.95 m (significant wave height)

where the angle is measured with respect to the range direction. The parameters of the best-fit simulated SAR

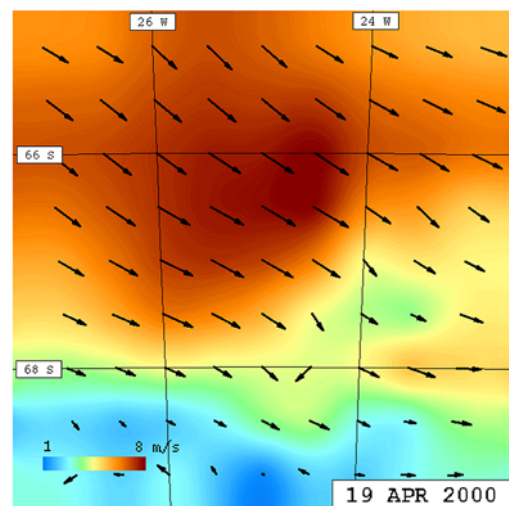


Figure 2. Gridded wind vectors extracted from QuikSCAT archive data for April 19, 2000, Time 12:00 UT.

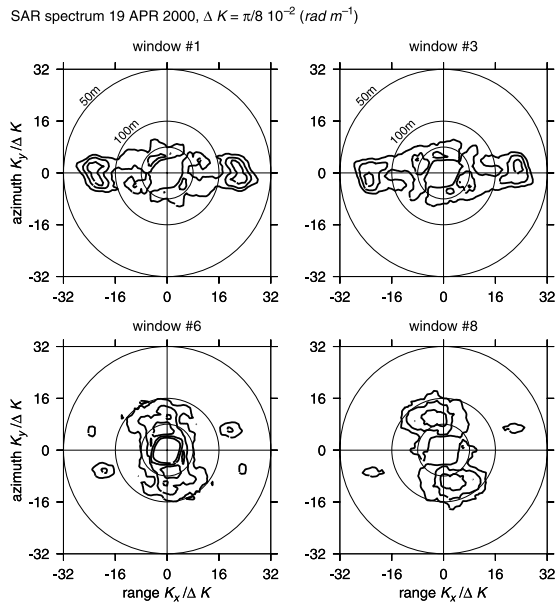


Figure 3a. Observed SAR spectra for 4 of the 8 windows of Figure 1, going from left (open sea) to right (sea ice).

spectrum, to be compared with the observed (in parentheses) SAR spectrum, are:

- Peak wavelength: 85.6 m (66.4 m)
- Peak wave direction: 16° (5°)

3.2. Sea Ice

[9] To invert the SAR image spectra in sea ice in order to infer physical properties such as thickness, a wave propagation model which accounts for wave dispersion and attenuation as a function of wave frequency and ice properties must be assumed. We use the Keller [1998] model, which treats the ice layer as a viscous fluid while the water beneath it is assumed inviscid. For deep water, the model has only two free parameters: the thickness and the ice viscosity. The idea is thus to find the best values of the two parameters which minimise the difference between the observed and simulated SAR spectra. It is assumed that the wave spectrum enters the ice edge and each wave component is attenuated according to the following expression to give the wave spectrum in sea ice:

$$S_{\text{ice}}(k) = S_w(k) \cdot \exp(-\alpha \cdot d), \quad (1)$$

where $S_w(k)$ is the wave spectral density in open sea, α is the attenuation rate computed by the model and d is the distance travelled by the wave from the ice edge. Since we are dealing with thin sea ice, it is assumed that the waves imaged by SAR (for wavelengths >50 m) cross the ice edge and their energy is transmitted without loss. In order to account for a change in the propagation of the wave components as a result of the ice edge crossing, it is assumed that the amount of rotation is independent of the wavelength. The latter feature is accounted for in the inversion algorithm as rigid rotation of the whole spectrum.

[10] The value 18.0 has been used as the modulus of RAR MTF in sea ice. It has been obtained using the procedure described in the open sea region. Although

slightly higher than the value found for open sea, it compares well with a value of 15 measured near the edge of frazil and pancake icefield in the Greenland Sea on ERS-1 SAR imagery taken on April 10 1993 [De Carolis, 2001]. Moreover, assuming that Bragg scattering is still the dominant microwave scattering mechanism in frazil-pancake ice, the slope n of the wave number spectrum (k^{-n}) lies between 7 and 8. The latter is an expected consequence of the ice sheet attenuation.

[11] The inversion procedure is once again parametric because two parameters (thickness h and kinematic viscosity ν) are to be retrieved. The algorithm is thus similar to the one implemented for wave spectrum retrieval in open sea. The retrieved ice parameters are:

$$c \cdot h = 24 \pm 1 \text{ cm (where } c \text{ is ice concentration)}$$

$$\nu = (5 \pm 1) \times 10^{-2} \text{ m}^2 \text{ s}^{-1}$$

These values are spatial averages over a distance up to 10–15 km from the ice edge.

[12] The best-fit ice parameters allow the computation of the attenuation rate $\alpha = \alpha(k)$ and hence of the wave spectrum in sea ice using (1). As a result, the following parameters relevant to the wave spectrum in sea ice were found:

- Peak wavelength: 80.6 m
- Dominant wave direction: 41°
- H_s : 1.65 m

The parameters of the best-fit simulated SAR spectrum, to be compared with the observed (in parentheses) SAR spectrum, are:

- Peak wavelength: 87.0 m (73.3 m)
- Peak wave direction: 22.4° (16.0°)

[13] It can be seen that the best fit for the kinematic viscosity is of the same order as the value found by Newyear and Martin [1999] in their tank experiments. Figure 3a shows the SAR spectra obtained from four of the eight subscenes. The change in shape of the spectrum after window 3, when the waves enter the ice, is very apparent, while at windows 6 and 8, about 16 km and 29 km inside the icefield, the high wave number components have almost disappeared. Figure 3b shows the full resolution SAR image windows on which the spectra of Figure 3a were computed.

4. Comparison With in Situ Data

[14] The intention of this experiment was to obtain SAR imagery directly overhead FS *Polarstern* as she launched an ice buoy array and carried out direct observations of frazil-pancake ice [Doble et al., 2003]. In the event, because of ice conditions, *Polarstern* was forced to carry out this work some 280 km to the west of the intended position, at $68^\circ 40'S$, $32^\circ 30'W$. However, the dates of the work (April 16–19) spanned the SAR overflight, and the composition of the MIZ appeared to be similar along the whole set of longitudes visited by *Polarstern*, being more a function of penetration from the ice edge than of geographical location. We therefore tentatively conclude that the ice sampled by *Polarstern* had the same characteristics as that seen on the SAR.

[15] The ice analysis was done as follows. Whole pancakes were lifted onto the deck and their dimensions measured; they were also cut up for salinity analysis. Frazil

ice in the interstices between pancakes was sampled by a tube covered at one end by a plankton net being lifted up through the suspension from beneath. Excess water was allowed to drain away then the ice sample was melted and the volume measured. The assumption was made, based on the observed ratios between measured ice volume and suspension depth seen in the original tube, that while in the water the frazil ice crystals within the suspension occupied a volume fraction of 0.4. Figure 4 shows the results of the sampling. The distributions of pancake and (corrected) frazil layer thicknesses are shown for all the stations, and for the outer and inner (greater than 70 km penetration) parts of the MIZ separately. Overall, 35 pancakes and 58 frazil samples were analysed. On the assumption of a 70% pancake fraction by area in the mix, the remainder being frazil, an overall mean thickness for the composite icefield was estimated at 24 cm. If the zones are considered separately the mean for the outer MIZ was 18 cm and for the zone at deeper penetration 32 cm.

5. Discussion of Results

[16] It was found that in the case studied, an excellent agreement between the optimised ice thickness (24 cm) and the mean of pancake ice thickness observations carried out concurrently in the marginal ice zone some 280 km to the west by FS *Polarstern* (also 24 cm) was obtained. The relevant optimal kinematic viscosity comes to $5 \times 10^{-2} \text{ m}^2 \text{ s}^{-1}$, which is in the range of laboratory values from *Newyear and Martin* [1999].

[17] The exactness of the agreement is, of course, fortuitous. The in situ mean thickness was based on averaging a finite number (93) of samples, and if we used data only from the outer zone of the MIZ, the mean thickness would be lower (18 cm). The SAR-derived thickness, although subject to an estimated technique-based error of only ± 1 cm, is also subject to unknown additional errors based on the imaging process. Yet the excellence of fit gives us valid grounds to propose that the SAR waves

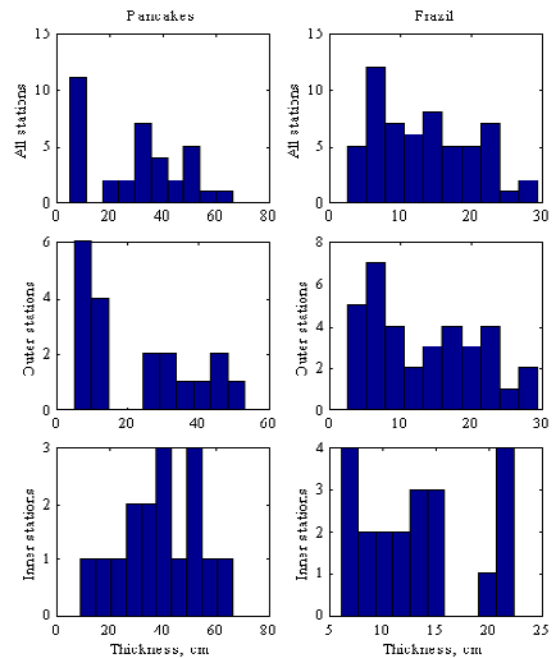


Figure 4. Distribution of measured thicknesses of pancakes and of frazil layers (assuming 0.4 frazil ice volume fraction) in samples taken by FS *Polarstern* in MIZ west of SAR site on April 16–19 2000. Results are shown for all stations and for the outer and inner MIZ separately.

technique combined with the Keller theory offers a powerful new tool for the remote sensing estimation of pancake icefield thicknesses. As well as being more accurate, the technique also has a finer resolution, since the mass loading method depended on detecting the change in wave number of the spectral peak (so that its lowest step was a unit based on the size of a pixel) whereas the new method optimises the change of shape of the whole spectrum.

[18] **Acknowledgments.** This work was supported by the Commission of the European Communities under contract EVK2-2000-00544 of the Environment and Climate Programme; by the Italian Space Agency (ASI) under contract 98–135; by the Italian Programme for Antarctic Research (P.N.R.A.); and by the Natural Environment Research Council of Great Britain under grant GR3/12592. We are grateful to the European Space Agency for the provision of ERS–2 SAR imagery. All images shown are copyright ESA.

References

- Baraldi, A., and F. Parmiggiani (1995), A refined gamma MAP SAR speckle filter with improved geometric adaptivity, *IEEE Trans. Geosci. Remote Sens.*, *33*, 1245–1257.
- De Carolis, G. (2001), Retrieval of the ocean wave spectrum in open and thin ice covered ocean waters from ERS synthetic aperture radar images, *Nuovo Cimento Soc. Ital. Fis. C*, *24*, 53–66.
- Doble, M. J., M. D. Coon, and P. Wadhams (2003), Pancake ice formation in the Weddell Sea, *J. Geophys. Res.*, *108*(C7), 3209, doi:10.1029/2002JC001373.
- Donelan, M. A., J. Hamilton, and W. H. Hui (1995), Directional spectra of wind generated waves, *Philos. Trans. R. Soc. London*, *315*, 509–562.
- Engen, G., and H. Johnsen (1995), SAR-ocean wave inversion using image cross spectra, *IEEE Trans. Geosci. Remote Sens.*, *33*, 1047–1056.
- Hasselmann, K., and S. Hasselmann (1991), On the nonlinear mapping of an ocean wave spectrum into a synthetic aperture radar image spectrum and its inversion, *J. Geophys. Res.*, *96*, 10,713–10,729.
- Hasselmann, S., C. Brüning, K. Hasselmann, and P. Heimbach (1996), An improved algorithm for the retrieval of ocean wave spectra from synthetic aperture radar image spectra, *J. Geophys. Res.*, *101*, 16,615–16,629.

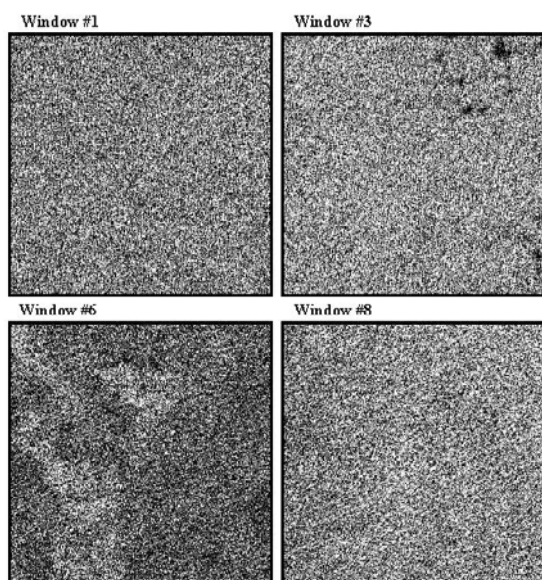


Figure 3b. Full resolution SAR image windows on which the spectra of Figure 3a were computed.

- Keller, J. (1998), Gravity waves on ice-covered water, *J. Geophys. Res.*, *103*, 7663–7669.
- Mastenbroek, C., and C. F. De Valk (2000), A semiparametric algorithm to retrieve ocean wave spectra from synthetic aperture radar, *J. Geophys. Res.*, *105*, 3497–3516.
- Newyear, K., and S. Martin (1999), Comparison of laboratory data with a viscous two-layer model of wave propagation in grease ice, *J. Geophys. Res.*, *104*, 7837–7840.
- Wadhams, P. (1986), The seasonal ice zone, in *The Geophysics of Sea Ice*, edited by N. Untersteiner, pp. 825–991, Plenum, New York.
- Wadhams, P., and B. Holt (1991), Waves in frazil and pancake ice and their detection in Seasat synthetic aperture radar imagery, *J. Geophys. Res.*, *96*, 8835–8852.
- Wadhams, P., F. Parmiggiani, G. de Carolis, and M. Tadross (1999), Mapping the thickness of pancake ice using ocean wave dispersion in SAR imagery, in *Oceanography of the Ross Sea Antarctica*, edited by G. Spezie and G. M. R. Manzella, pp. 17–34, Springer-Verlag, New York.
- Wadhams, P., F. Parmiggiani, and G. de Carolis (2002), The use of SAR to measure ocean wave dispersion in frazil-pancake icefields, *J. Phys. Oceanogr.*, *32*, 1721–1746.
-
- G. de Carolis, Istituto di Studi sui Sistemi Intelligenti per l'Automazione, Consiglio Nazionale delle Ricerche (ISSIA-CNR), via Amendola 122/D, 70126 Bari, Italy.
- D. Desiderio, Carlo Gavazzi Space SpA, via Gallarate 150, 20151 Milan, Italy.
- M. J. Doble and P. Wadhams, Scottish Association for Marine Science, Dunstaffnage Marine Laboratory, Oban PA37 1QA, Scotland. (p.wadhams@sams.ac.uk)
- F. F. Parmiggiani, Istituto di Scienze dell'Atmosfera e del Clima, Consiglio Nazionale delle Ricerche (ISAC-CNR), via Gobetti 101, 40129 Bologna, Italy.